Available online at www.sciencedirect.com
ScienceDirect
International Journal of Heat and Mass Transfer 49 (2006) 4786–4794
International Journal of HEAT and MASS TRANSFER
www.elsevier.com/locate/ijhmt

Numerical simulation of the He II/He I phase transition in superconducting magnets

Shaolin Mao [a,*], Cesar A. Luongo [b], David A. Kopriva [c]

[a] Department of Mechanical Engineering, Tulane University, New Orleans, LA 70118, USA
[b] National High Magnetic Field Laboratory, Florida State University Tallahassee, FL 32310, USA
[c] Department of Mathematics, Florida State University Tallahassee, FL 32304, USA

Received 30 December 2005; received in revised form 3 June 2006
Available online 5 September 2006

Abstract

In this paper we simulate a special type of Stefan problem in large-scale superconducting magnet systems in which superfluid helium (He II) is used as the coolant for the system. Liquid helium in a narrow channel called a "cable-in-conduit" conductor (CICC) is used to remove the heat load from the conductors. Liquid helium exhibits a phase change transition to normal helium (He I) when its temperature rises above the lambda point (2.716 K under saturated vapor pressure). A simple one-dimensional model is described to analyze this special He II/He I Stefan problem. A moving mesh technique is used to solve this model to improve the numerical efficiency compared with front-tracking methods. The results illustrate the simplicity and efficiency of this model.

Keywords: Stefan problem; Moving grid method; Enthalpy method

1. Introduction

The 45-Tesla Hybrid Magnet System of the National High Magnetic Field Laboratory (NHMFL) provides researchers with the highest steady DC magnetic field available anywhere in the world today [1,2]. The superconducting magnet was designed with superfluid helium (He II) as the coolant and the magnet coils are wound with a special type of conductor, namely, a cable-in-conduit conductor (CICC). Stainless steel is used as the conduit to contain the coolant and support mechanical loads (large Lorentz force produced by the high magnetic field), superconducting strands are set inside the conduit, and stagnant superfluid helium fills the interstices inside of the conduit [1]. The temperature of the superfluid helium in the cryostat vessel is set to 1.6–1.8 K [2,3]. The superfluid helium exhibits very special properties, such as excellent thermal conductivity (~1000 times of that of copper), no viscosity under certain conditions, and Gorter–Mellink law of heat conduction etc., [8]. Because of the high cost associated with the design and construction, the magnet system is designed from the outset as a user facility rather than experimental equipment. Due to the difficulties of effective and accurate measurement of the temperature and pressure in the CICC channel, modeling of the flow and heat transfer of helium is an important aspect during design. Of particular importance is the simulation of "quench", the sudden loss of superconductivity, an event requiring special protective measures in any large-scale magnet. Development of numerical model for superfluid helium stems from the need for accurate analysis of the thermal processes in the CICC to better explain the observations from coil voltage taps and various external temperature sensors and pressure transducers.

In the past decades, most analytical, numerical, or experimental works on superfluid helium flow and heat transfer has focused on smooth rectangular chambers or channels [4–7]. Kashani et al. [8] simulated 1D forced

* Corresponding author. Present address: Tulane University, New Orleans, LA 70118, USA. Tel.: +1 504 865 5178; fax: +1 504 865 5345.
E-mail address: smao@tulane.edu (S. Mao).

0017-9310/$ - see front matter © 2006 Elsevier Ltd. All rights reserved.
doi:10.1016/j.ijheatmasstransfer.2006.06.004

convection heat transfer in He II in a smooth channel. Kitamura et al. [9] used a 2D model to analyze transient heat transfer in He II. Ueta et al. [10] experimentally demonstrated the λ-phase transition between He II and He I induced by shock compression. Tatsumoto et al. [11,12] obtained 2D simulation results of steady-state and transient heat transfer of He II in a duct. Due to the complicated structure in the CICC, reports of numerical or experimental results on flow and heat transfer in He II are very scarce. Bottura et al. [13] used a quasi-1D model to simulate He II flow and heat transfer in the CICC. Mao et al. [14] analyzed the λ-phase transition between He II and He I in the CICC. Accurate simulation of the λ-phase transition depends on two aspects. First, precise evaluation of a wide range of heat load such as AC losses, joint losses, and index heating which are deposited to liquid helium [3,15]. Second, an effective method is needed to track the helium λ-phase transition correctly.

The helium λ-phase transition (He II/He I moving front) problem can be regarded as a special liquid/liquid phase transition. The transition is a second-order phase transition without latent heat, which means there is no discontinuity in the entropy across the λ-phase line [16]. Further, the specific heat of liquid helium has a logarithmic infinity at the λ-phase temperature T_λ. However, the enthalpy of helium is continuous cross the lambda point.

There are a number of numerical algorithms available to deal with moving boundary problems, such as front-tracking methods [17], fixed grid methods [18], and phase field method [19]. Front-tracking methods need to calculate the phase change fronts explicitly at each time step. Interpolation is usually used near the fronts. It is straightforward, but it may sometimes be difficult or even impossible to track the moving front directly. The Enthalpy method is a kind of fixed grid method that avoids calculating the moving front explicitly. The position appears, *a posteriori*, is a key feature of this method. Phase field methods, based on Landau–Ginzburg theory instead of the enthalpy function, avoid the need to explicitly track the moving interface by front-track methods. In this paper a simple enthalpy method is used to solve the He II/He I moving front problem.

The objective of this study is to apply a moving grid algorithm that uses the enthalpy method to improve the computing efficiency of the simulation of the He II/He I transition. In order to obtain high resolution, a large number of mesh points is required in the high gradient region. The mesh does not need to be as fine far away from the interface where the temperature is smooth. A simple physical model will be introduced in Section 2, a moving mesh method is described in Section 3, followed by numerical implementation and simulation results in Sections 4 and 5.

2. Modeling of helium transition in a CICC

The behavior of superfluid helium (He II) has been modeled as a mixture of superfluid component and normal fluid component, called a two-fluid model. The superfluid component carries no entropy and has no viscosity. As the temperature decreases the concentration of superfluid component increases so that at 1 K the normal fluid constitutes only 1% of the total [8]. In many engineering applications involving He II, this two-fluid model can be simplified by assuming single phase that is separated by the helium transition point, namely, the lambda temperature T_λ. In the CICC channel, the time evolution of the temperature of the conductors and liquid helium and the He II/He I transition are our main interests. Basic assumptions about the flow are made as follows [14]:

(1) Only one-dimensional heat conduction along the longitudinal direction is considered. This is a reasonable approximation for the large length/diameter ratio of a CICC,
(2) Convection effects are neglected. The helium is stagnant initially and flow induced by the heat disturbance is relative small during the He II/He I phase transition,
(3) The influence of gravity is neglected,
(4) He II has excellent thermal conductivity; the contribution from conductors (superconductor plus copper) are not taken into account in He II region,
(5) He I has very poor heat conductivity; the copper (conductor) is the main contribution to the conduction of heat when the temperature is above the lambda point, and
(6) Very good insulation between layer-to-layer or turn-to-turn of coils in magnets in which it is a reasonable choice to apply 1-D pipe filled with stagnant helium to analyze thermal behavior of wound solenoids.

The heat conduction in He II obeys the Gorter–Mellink law [16], viz.:

$$q_x = -K(\mathrm{d}T/\mathrm{d}x)^{1/3} \tag{1}$$

where $K = (f^{-1}(T,p))^{1/3}$ is the equivalent thermal conductivity of He II that can be written as a function of temperature and pressure.

The energy balance adding the corresponding heat generation terms becomes [14]:

$$\rho c \frac{\partial T}{\partial t} = \frac{\partial}{\partial x}\left[K_{\mathrm{He}}\left(\frac{\partial T}{\partial x}\right)^{1/3}\right] + q(x,t) \quad T < T_\lambda \tag{2}$$

$$\rho c \frac{\partial T}{\partial t} = \frac{\partial}{\partial x}\left[\frac{A_{\mathrm{Cu}}}{A} K_{\mathrm{Cu}} \frac{\partial T}{\partial x}\right] + q(x,t) \quad T_\lambda \leqslant T \tag{3}$$

$$\rho_{\mathrm{He}} \Delta c_{\mathrm{He}} \frac{\mathrm{d}s(t)}{\mathrm{d}t} + K_{\mathrm{Cu}} \frac{\partial T}{\partial x} = -K_{\mathrm{He}}\left(\frac{\partial T}{\partial x}\right)^{\frac{1}{3}} \tag{4}$$

$$T(0,t) = T(l,t) = T_{\mathrm{b}}, \quad T(x,0) = T_{\mathrm{b}} \tag{5}$$

$$T(s(t),t) = T_\lambda \tag{6}$$

where the subscript $[\,]_{\mathrm{Cu}}$ and $[\,]_{\mathrm{He}}$ refer to copper in the conductor and helium, respectively, $q(x,t)$ is the source including the AC losses, the index heating, and the heat transfer

between two adjacent CICCs. The term $s(t)$ refers to the location of the He II/He I front. Δc_{He} is the difference of helium specific heat across the front. For the regions where the temperature goes above the lambda point, the energy balance equation becomes a classic Fourier heat conduction. The term ρc represents the equivalent heat capacity of liquid helium plus copper. Its definition is $\rho c = A_{He}(\rho c)_{He}/A + A_{Cu}(\rho c)_{Cu}/A$. T_b is the clamped helium bath temperature (1.8 K), and T_λ is the superfluid transition (2.176 K under saturated vapor pressure). In the absence of heat generation due to compressibility or viscous dissipation, Eqs. (2)–(6) are suitable for the description of a Stefan phase change problem [17].

The heat balance Eq. (4) is required for several reasons. First, a new variable $s(t)$ is introduced explicitly. Secondly, a very special property shown in Eq. (4) is that the heat capacities are not continuous when crossing the λ-phase transition. Third, the large "jump" of heat capacities of helium across lambda point requires accurate estimation of He II/He I front. Even though Eqs. (2) and (3) are physically proper definite with well-posed initial and boundary conditions, the main concern in this study is to improve the resolution of He II/He I front without losing of computational efficiency. On the moving front, the temperature is fixed (because of constant pressure) and the Stefan condition (4) is satisfied for the heat balance. The jump in the heat capacities of the helium, $\rho_{He}\Delta c_{He}$, makes it difficult to evaluate the moving front accurately. The enthalpy method is used to avoid solving the Stefan condition explicitly, as it was done in the front-tracking method before [14].

The use of the enthalpy method has a detailed introduction by Crank [17] and other researchers [20,21]. The procedure is to introduce an enthalpy or the total heat content function, $H(T)$ that consists of the specific sensible heat and the latent heat required for a phase change. The definition of the enthalpy function is:

$$H(T) = \begin{cases} \int_{T_0}^{T} c_{\text{He-II}}(\theta)\,\mathrm{d}\theta & T < T_\lambda \\ \int_{T_0}^{T} c_{\text{He-I}}(\theta)\,\mathrm{d}\theta & T_\lambda < T \end{cases} \tag{7}$$

where c_{He} is not continuous crossing the lambda point T_λ. The enthalpy definition by Eq. (7) is under constant pressure condition which corresponds to the specific enthalpy of helium in this study. The values of specific enthalpy of helium under constant pressure can be obtained from a computer code HEPAK [25]. The He II/He I moving front problem (2)–(4) can be recast as a single equation in terms of the specific enthalpy:

$$\rho\frac{\partial H}{\partial t} = \nabla\cdot(K\nabla T) + q(x,t) \tag{8}$$

where $K = \begin{cases} K_1 & T < T_\lambda \\ K_2 & T_\lambda < T \end{cases}$. The thermal conductivity K_1 is used by Bottural et al. [13] analogously to the classic Fourier thermal conductivity. The enthalpy function in the definition (7) differs from the conventional definition, which includes the latent heat term [18,20]. The biggest advantage of the enthalpy method is that it avoids the main difficulty of front-tracking methods. Instead, the position of the moving boundary has to be determined in retrospect by inspection of the computed values of H and T.

Eqs. (7) and (8) represent a one-dimensional, two-fluid model from which the temperature evolution in the CICC can be calculated. It is a non-linear system of partial differential equations requiring numerical solution.

3. Moving grid method

There are several ways to improve the accuracy of the enthalpy method; the moving grid method is adopted in this paper. The success of any numerical solution of moving front problems requires that the interfacial region be well resolved. The computational grid mesh does not need to be fine uniformly the computational domain. Moving grid methods are relatively easy to implement and a good way to improve the accuracy of the solution in steep gradient regions. The computation of the grid points is based on the equidistributing principle [21]. In practice, a monitor function is chosen to follow the change of the solution over time. A popular selection for problems with steep gradients is a scaled arc-length function of the solutions such as [22],

$$M(x) = \sqrt{1 + \alpha\left(\frac{\partial H}{\partial x}\right)^2} \quad \alpha > 0, \tag{9}$$

where α is a user-chosen parameter. Unfortunately this function is not analytical integrable and unsuitable for multi-phase problems. Hence, this equidistribution principle has to be approximated using quadratures. So we consider to equidistribute according to the monitor function [23]:

$$M(x) = 1 + \frac{\mu_1}{\sqrt{\mu_2^2(x-s)^2 + 1}}. \tag{10}$$

where the parameters μ_1 and μ_2 are positive constants to control the smoothness and clustering of the grid around the front $s(t)$. The function (10) is analytically integrable and the set of grid points $\{x_j\}$ is the solution of the following scalar non-linear equations [24]:

$$\begin{aligned} &x_j + \frac{\mu_1}{\mu_2}\sinh^{-1}(\mu_2(x_j - s)) - \frac{\mu_1}{\mu_2}\left(1 - \frac{j}{N}\right)\sinh^{-1}(\mu_2(x_L - s)) \\ &\quad - \frac{j}{N}\left((x_R - x_L) + \frac{\mu_1}{\mu_2}\sinh^{-1}(\mu_2(x_R - s))\right) = 0 \\ &\quad \text{for } j = 1, 2, \ldots, N-1. \end{aligned} \tag{11}$$

The solution of (11) is a trivial step; for example, it can be solved using Newton–Raphson iterative method. The advantage of this choice of the monitor function is that it gives rise to smooth mesh trajectories and automatically clusters mesh points around steep gradient regions.

4. Numerical algorithm

There are several choices of numerical discretization approaches to solve Eqs. (7) and (8), such as Galerkin weighted residual finite element method, finite volume method and finite difference method. We apply the Method of lines (MOL) on spatial derivatives and forward Euler scheme to solve the ordinary differential equations (ODEs) obtained from MOL in time. To this point, we choose central finite difference in space. In order to incorporate the moving grid method a semi-Lagrangian formulation of Eq. (8) is written in the form:

$$\dot{H} - \dot{x}\frac{\partial H}{\partial x} = \frac{\partial}{\partial x}\left(K\frac{\partial T}{\partial x}\right) + q(x,t) \tag{12}$$

where $\dot{H}$ and $\dot{x}$ denote the derivatives with respect to time in a Lagrangian coordinate frame. A constant time step and adaptive grid size are denoted by $\Delta t = t^n - t^{n-1}$ and $h_j^n = x_j^n - x_{j-1}^n$. Therefore Eq. (12) is explicitly discretized as:

$$\frac{H_j^{n+1} - H_j^n}{\Delta t} - \frac{x_j^{n+1} - x_j^n}{\Delta t}\left(\frac{H_{j+1}^n - H_{j-1}^n}{h_{j+1}^n + h_j^n}\right) = \frac{2}{h_{j+1}^n + h_j^n}\left(K_{j+1}^n\frac{T_{j+1}^n - T_j^n}{h_{j+1}^n} - K_j^n\frac{T_j^n - T_{j-1}^n}{h_j^n}\right) + q_j^n \tag{13}$$

Dirichlet boundary conditions are imposed at the two ends $x = x_L$ and $x = x_R$ namely:

$$T_0^{n+1} = T_b \tag{14}$$

$$T_N^{n+1} = T_b \tag{15}$$

and Eq. (13) are applied for $j = 1,\ldots,N-1$. The complete algorithm is to solve (11) and (13) at each time step simultaneously as a large algebraic system. A more efficient approach is to solve the mesh Eq. (11) independently. Decoupling enables the use of iterative methods with different tolerances to determine the grid and solution. A complete algorithm is given as follows:

(1) Predict the initial position of the moving front. The initial condition of the He II/He I phase change problem is $s(t=0) = 0$.
(2) Solve mesh Eq. (11) to obtain the grid points $\{x_{j,s}^{n+1}\}$.
(3) Solve the governing Eq. (13) for temperature $\{T_{j,s}^{n+1}\}$, and then determine the moving front position $s_{\Delta,s+1}$ by linear interpolation for the temperature T_λ.
(4) Compare the tolerance of the front position at two adjacent iterations; otherwise go to step (2).

This algorithm avoids solving the Stefan condition explicitly. The iteration procedure is also straightforward. Usually the tolerance of the mesh iteration is set to 10^{-3}. More discussions for the convergence of the solution for Stefan problems can be found in Crank [17].

5. Numerical results and discussion

In this paper we discuss a helium evolution problem in which the CICC channel is presumed to be symmetric about the origin, and we only perform the analysis on half of the CICC. In this study, we simulate coil "A" of superconducting outset of 45-T hybrid magnet system. Dimensions of CICC and other mechanical parameters can be found in [3]. To compare the numerical results with other methods such as the front tracking method [14], 400 grid points were used to discretize the channel with length of 114.7 m. Time step is determined by the numerical stability of explicit schemes and the accuracy requirement for parabolic problems with large non-linear source terms. The time step is fixed $\Delta t = 1.0 \times 10^{-5}$. To test the convergence of the numerical solution a $\Delta t = 5.0 \times 10^{-6}$ is also use for moving grid method and front-tracking method. The minimum mesh size in moving grid method is in the same order of magnitude with that for front-tracking method. The smaller size of meshes the more accurate the moving front tracking. The initial and boundary conditions are given as follows:

$$T_b = 1.8\,\mathrm{K},\ T(x,0) = 1.8\,\mathrm{K},\ s(x,0) = 0,$$
$$A_{Cu}/A = 54.25\,\mathrm{mm}^2/104.55\,\mathrm{mm}^2 = 0.519$$
$$L = 114.7\,\mathrm{m},\ \dot{I} = 2.5\text{–}5.0\,\mathrm{A/s},\ T_\lambda = 2.168\,\mathrm{K},\ B_{max} = 15.3\,\mathrm{T},$$
$$I_{max} = 10\,\mathrm{kA},\ P = 1.0\times10^5\,\mathrm{Pa},\ v = 0.0\,\mathrm{m/s}$$

In the above, pressure is constant and $T_\lambda = 2.168K$ is the helium Lambda point under 0.1 MPa pressure. The density, specific heat, thermal conductivity, and enthalpy of helium are all temperature-dependent and highly nonlinear parameters. They are computed using the computer code HEPAK [25]. Fig. 1 shows that the enthalpy of helium is continuous through the He II/He I front (the λ-transition), but exhibits a jump at the boiling temperature of helium (4.22 K at 0.1 MPa pressure) because of the latent heat of helium. Fig. 2 shows a large gradient in the heat capacity of the helium across the He II/He I front, which makes the computation difficult. Effective front-tracking needs a discretization of the first and second derivatives across the He II/He I front, otherwise large numerical errors and numerical uncertainties are produced. The enthalpy method used here computes the He II/He I front *a posteriori*. It overcomes the numerical difficulty of discretization of the heat balance equation for the He II/He I front.

The evolution of helium temperature and He II/He I transition depends on the external heat deposited to the helium. Two main heat sources in a CICC channel are the AC losses and index heating, both of which are nonlinear functions of the magnetic field B and the operating current I. The AC losses stem from the change of operating electric current in the conductor while index heating is an exponential function of the ratio of operating current vs. critical current of the conductor. Different current ramping

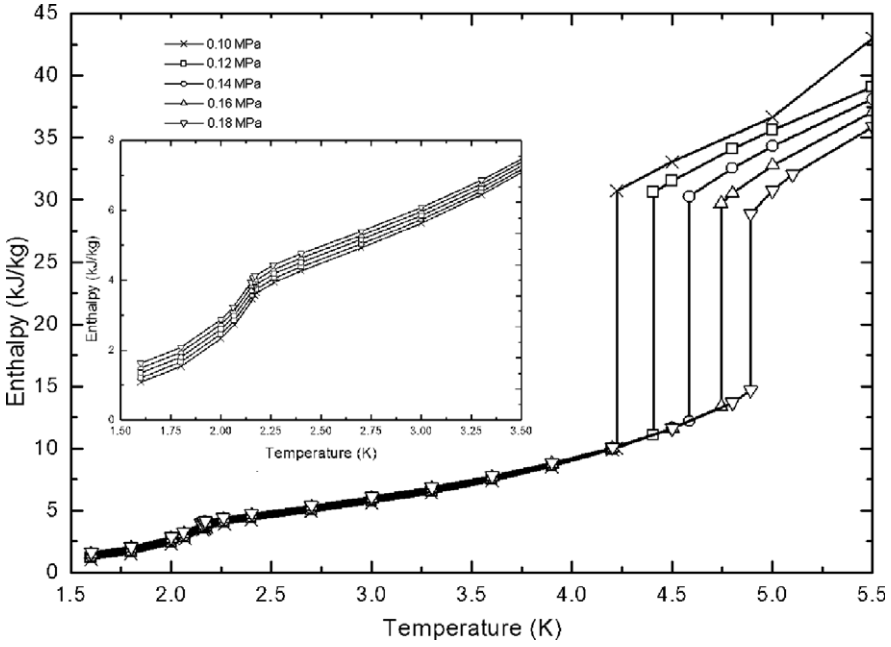

Fig. 1. The enthalpy of helium as a function of temperature and pressure is continuous across the lambda point (2.168 K at 0.1 MPa pressure in the inset diagram) and has a discontinuity (latent heat) at the boiling point (4.22 K at 0.1 MPa pressure).

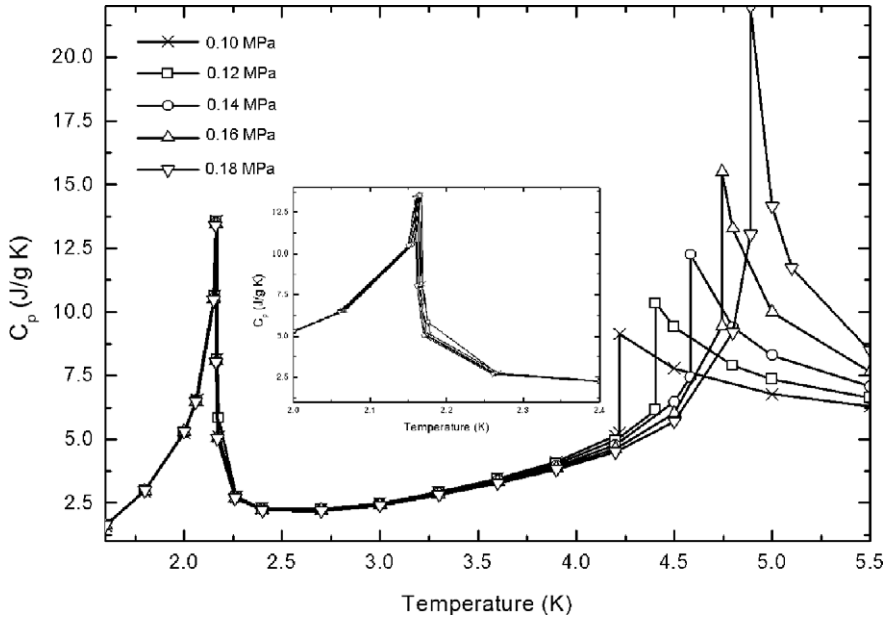

Fig. 2. The specific heat of helium at a constant pressure as a function of temperature. Two discontinuities appear across the λ-point (He II/He I) and the boiling point (supercritical Helium).

rates produce different AC losses. The operating current is set up to 10 kA. The AC losses become largest at $t = 500$ s for a 2.5 A/s ramping rate. The heat generation rate is up to a maximum value of 0.0122 w/m at the innermost layer of coil "A". AC losses decrease after 500 s and become zero if the current ramping process ends [15]. At the initial time, the CICC channel is assumed to have static He II everywhere, and a constant temperature (1.8 K) cryostat vessel is connected to the CICC channel (the helium pressure is a constant that is adjustable through valves).

Figs. 3 and 4 show the evolution and distribution of the helium temperature in a CICC channel under the He II phase. At the early time the electrical current and the magnetic field are small ($t < 100$ s), and the AC losses increase slowly. Fig. 3 shows that the temperature at the middle increases first and slowly propagates to the ends of the CICC channel. After 200 s the AC losses increase rapidly because of the increase in the magnetic field and the electrical current. The large heat source accelerates the increase of the temperature of the He II ($t = 200$ s and $t = 300$ s

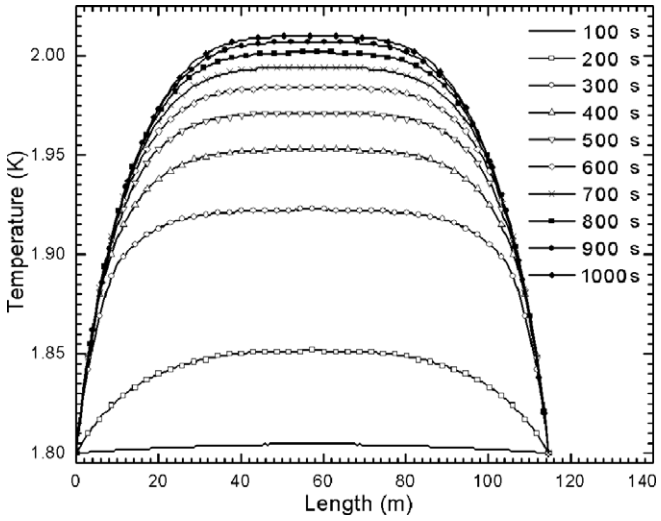

Fig. 3. The distribution and history of helium temperatures below the lambda point at the earlier ramping procedure, and the current ramping rate is 2.5 A/s.

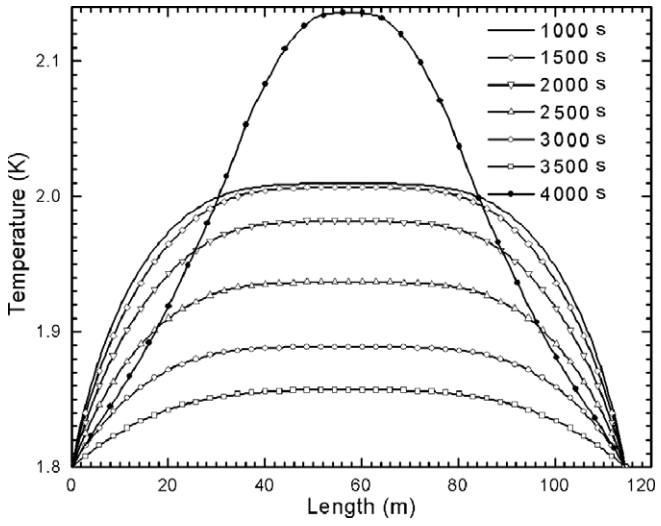

Fig. 4. The distribution and history of helium temperatures below the lambda point at the middle ramping procedure where the current ramping rate is 2.5 A/s.

in Fig. 3). The evolution of the He II temperature becomes slower after $t = 500$ s than that at $t = 200$ s due to the decrease in AC losses and a larger heat capacity of He II near the lambda point. Fig. 4 shows that the temperature of He II decreased with time ($t < 4000$ s). Due to the decrease of the heat deposit, the amount of heat removed by the He II surpasses that deposited by external heat sources. The cooling system is still in the safe zone and will retain the initial condition if current ramping ends at $t = 3500$ s (Fig. 4). At the later time the operating current becomes very large and the AC losses are small. However, the index heating cannot be negligible. The index heating is the main heat "load" to drive the temperature of the He II upward again (see the line $t = 4000$ s in Fig. 4). The system is more sensitive to heat capacities of helium at this stage.

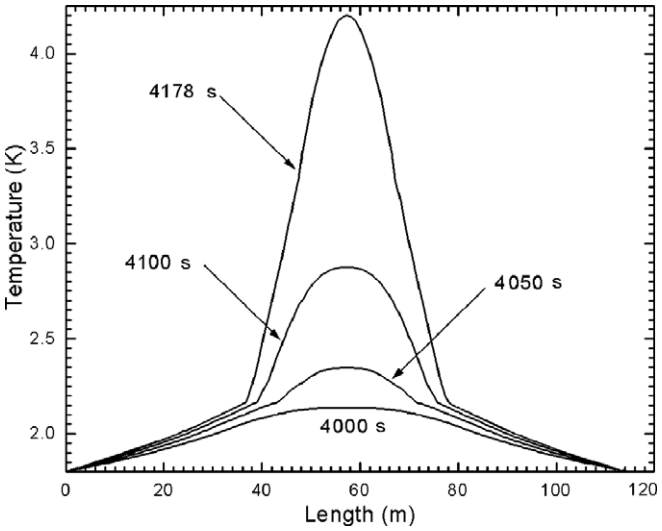

Fig. 5. The evolution of helium temperature in the CICC channel showing, helium temperature increases very quickly above the lambda point. It is clear that the He II/He I phase change fronts are moving towards the two ends.

Fig. 5 shows the λ-transition of helium temperature after the operating current reaches 10 kA (a ramping rate of 2.5 A/s is used) for the superconducting magnet system. The temperature of He II increases, and the degradation of heat conduction makes the system more unstable. The helium temperature gives rise to values above the lambda point in the middle position first, and He II transforms to He I. The figure shows a clear He II/He I phase front during the transition (the pressure is a constant at the cryostat and the temperature $T_\lambda = 2.168$ K under 0.1 MPa of pressure). Due to very poor heat conductivity of the He I, the removal of the heat load depends on the copper in the CICC channel; the rate of accumulation is faster than the rate of removal from the system. The helium temperature goes up faster than that in the single He II phase. As the helium temperature rises above 4.22 K (under 0.1 MPa of pressure), the heat transfer enters the boiling phase, and the system will lose its thermal stability completely. When the electrical current ramping process is faster than its stability margin, the helium cannot remove the heat deposition from the two ends of the CICC channel, which makes the situation more impaired. It is very important to note that two symmetrical He II/He I moving fronts are speeding up to the ends because more and more He II changes to He I in the CICC channel. Fig. 5 shows that the propagation of this He II/He I front could reach to 0.11 m/s even higher.

Figs. 6 and 7 demonstrate the grid tracking of the He II/He I front during the temperature evolution in the CICC channel. It demonstrates that the grid points are smoothly advancing with the physical solutions. Two parameters, μ_1 and μ_2, are used to adjust the clustering and smoothness of the grid points. Larger μ_1 results in a denser distribution of grid points with which to track the He II/He I front. Therefore the moving grid method can improve the efficiency of tracking the moving front. Otherwise a complicated

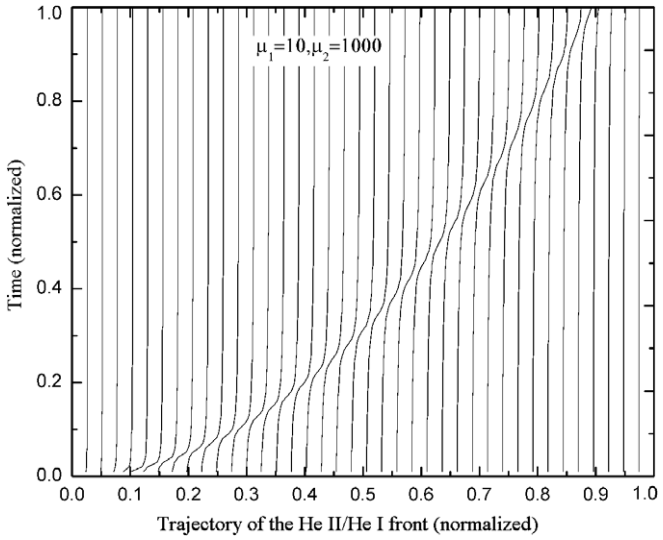

Fig. 6. The trajectory He II/He I moving front by the moving grid method: $\mu_1 = 10$, and $\mu_2 = 1000$.

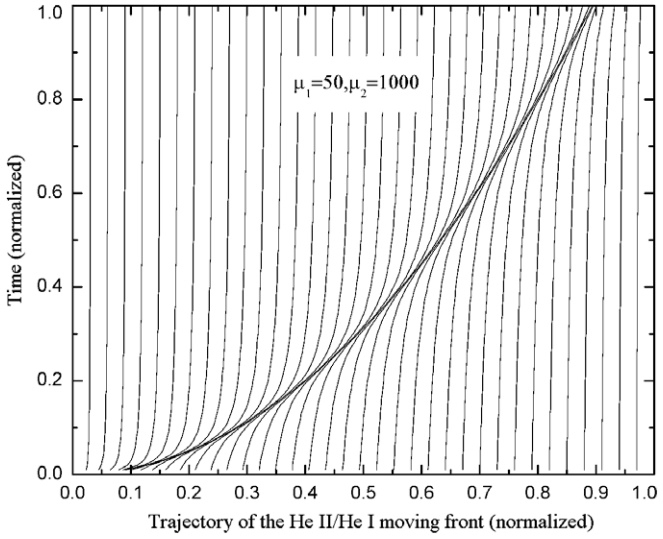

Fig. 7. The trajectory He II/He I moving front by the moving grid method: $\mu_1 = 50$, and $\mu_2 = 1000$. More grid points are concentrating near the moving interface.

adaptive mesh refine (AMR) is required in front-tracking methods. The overhead of this moving mesh method is an additional grid equation to be solved at each time step.

The trajectories of the He II/He I moving front are recorded from the beginning (He I first occupied in the middle position of the channel) to the time when He I fills 90% of the channel. The numerical results also show that the He II/He I front is moving non-linearly to the ends of the CICC channel in several tens of seconds. The moving front propagates faster at the early phase than that at the later phase. A possible reason is that constant pressure and clamped He II temperature are assumed at the ends, and this acts as a large reservoir or buffer to absorb the huge quantity of heat from the He I region. When the moving front approaches the end of the channel (90% of the

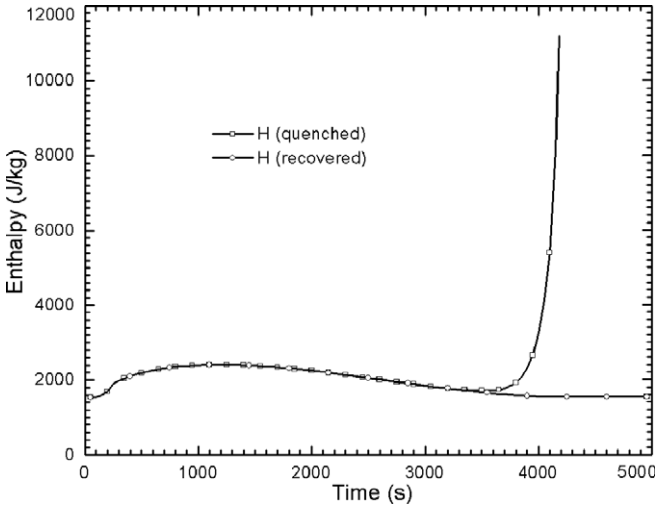

Fig. 8. Comparison of two runs for the recovery and runaway ("quench") of helium in the CICC channel. The recovery time is more than 1 h and less than one and a half hour.

channel is occupied with He I), the propagation of He II/He I becomes slower and the helium temperature in the central area of the channel rises rapidly.

Fig. 8 shows two runs showing the evolution of the helium enthalpy. One run is in the thermal stability margin. There, the helium enthalpy decreases as before because of the powerful heat transfer ability of He II. The recovery time is more than one hour and less than one and a half hours, which is in very good agreement with practical observation [3]. As the external heat surpass the thermal stability margin, He II changes to He I and the cooling ability degenerates. This results in quench of the superconductors. Fig. 9 gives a detail explanation of a thermal stability margin. When the external disturbance is large, the temperature of helium rises to a value above the λ-point, even after the conclusion of the electrical current ramp. The external heat (index heating) continues pushing the temperature rise, and finally arrives at the liquid/vapor line

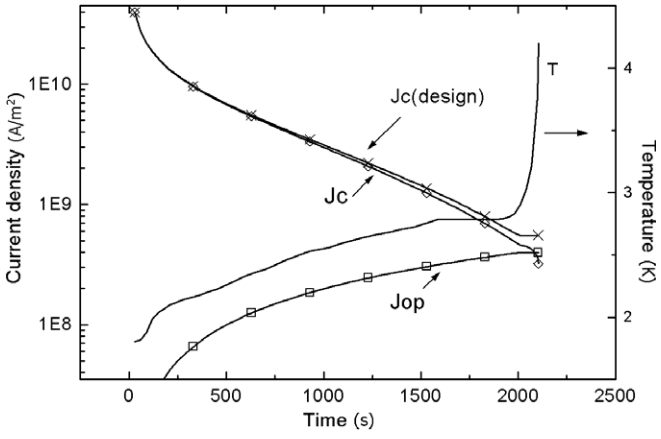

Fig. 9. The temperature evolution providing an explanation of the thermal stability of He II cooled magnets in the presence of current ramping (J_c: critical current density, J_{op}: operating current density).

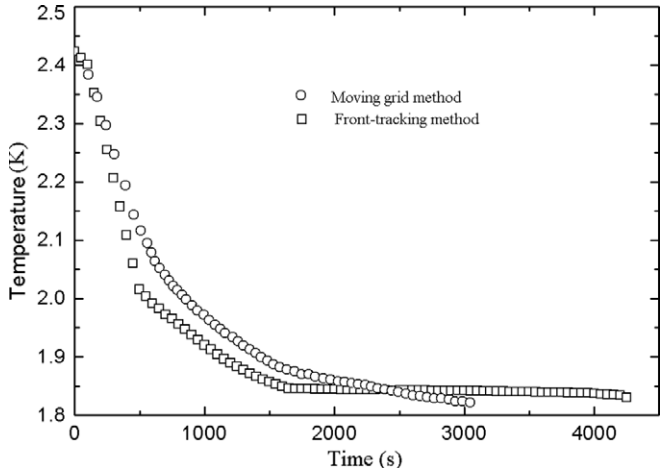

Fig. 10. The recovery of helium temperature by the front-tracking method and the moving grid method. Experimental observation is that it takes 30–35 min (1800–2100 s) to go back to normal operating temperature (1.8 K).

of helium (4.22 K under 0.1 MPa of pressure) and the system cannot recover any more.

Fig. 10 shows the recovery time of the helium temperature by two methods: front-tracking and moving grid techniques. As the helium temperature is driven above the λ-point, all external heat sources are removed and the system will return to its original state. Four thousand seconds, or 1 h and 15 min later, the temperature goes back to 1.83 K (the cryostat is fixed at 1.8 K) by the front-tracking method. It takes only 50 min for the temperature to decrease to 1.825 K when moving grid method is used. The actual operating observation shows that in 35–40 min the system can completely recover to its initial condition. This suggests that the enthalpy method used with the moving grid technique can obtain higher accuracy than tracking the He II/He I front by a front-tracking method.

6. Conclusion

A simple and efficient helium transient heat transfer model in a CICC has been proposed and implemented. Numerical experiments were carried out to study the evolution behavior of the temperature of the conductors and He II/He I moving fronts. The enthalpy method and an analytically integrable moving grid technique are used to improve the resolution of the He II/He I front. It avoided tracking the He II/He I front explicitly. The method improved the solutions that arise due to the difficulties and inaccuracies of calculation of the specific heat of liquid helium. The simulation results are compared to experimental observations and are shown to be in very good agreement. The merits of this model are its simplicity and ability to correctly track the temperature evolution of the column of helium in the CICC, without the complicated computation of the helium flow and coupled heat transfer between solid materials and the liquid helium.

Acknowledgement

The research was partially supported by the Center for Advanced Power Systems, Florida State University, with funding from the Office of Naval Research (ONR).

References

[1] M.N. Wilson, Superconducting Magnets, Clarendon Press, Oxford, 1983.
[2] J.R. Miller, S.W. Van Sciver, H.J. Schneider-Muntau, An overview and status of the NHMFL 45-T hybrid project, Teion Kogaku 31 (5) (1996) 240–249.
[3] J.R. Miller, Y.M. Eyssa, S.D. Sayre, C.A. Luongo, Analysis of observations during operation of the NHMFL 45-T hybrid magnet system, Cryogenics 43 (3) (2003) 141–152.
[4] L. Dresner, Transient heat transfer in superfluid helium, Adv. Cryo. Eng. 27 (1982) 411–419.
[5] L. Dresner, Transient heat transfer in superfluid helium – part II, Adv. Cryo. Eng. 29 (1984) 323–333.
[6] P. Seyfert, J. Lafferranderie, G. Claudet, Time-dependent heat transfer in sub-cooled superfluid helium, Cryogenics 22 (1984) 401–408.
[7] S.W. Van Sciver, Heat transfer in forced flow He II: Analytic solution, Adv. Cryo. Eng. 29 (1984) 315–322.
[8] A. Kashani, S.W. Van Sciver, J.C. Strikwerda, Numerical solution of forced convection heat transfer in He II, Numer. Heat Transfer: Part A 16 (1989) 213–228.
[9] T. Kitamura, K. Shiramizu, N. Fujimoto, Y.F. Rao, K. Fukuda, A numerical model on transient, two-dimensional flow and heat transfer in He II, Cryogenics 37 (1997) 1–9.
[10] Y. Ueta, K. Yanaka, M. Murakami, H. Nagai, H.S. Yang, Experimental study of λ-phase transition induced by shock compression, Cryogenics 42 (2002) 645–651.
[11] H. Tatsumoto, K. Fukuda, M. Shiotsu, Numerical analysis for steady-state two-dimensional heat transfer from a flat plate at one side of a duct containing pressure He II, Cryogenics 42 (2002) 9–17.
[12] H. Tatsumoto, K. Fukuda, M. Shiotsu, Numerical analysis for two-dimensional transient heat transfer from a flat plate at one side of a duct containing pressure He II, Cryogenics 42 (2002) 19–28.
[13] L. Bottura, C. Rosso, Finite element simulation of steady state and transient forced convection in superfluid helium, Int. J. Numer. Meth. Fluids 30 (1999) 1091–1108.
[14] S. Mao, C.A. Luongo, J.R. Miller, Analysis of the NHMFL 45-T hybrid magnet thermal behavior, Cryogenics 43 (3) (2003) 153–163.
[15] S. Mao, C.A. Luongo, J.R. Miller, Investigation of Index Heating as Source of Quench in the NHMFL 45-T Hybrid Superconducting Outsert, IEEE Trans. Appl. Supercond. 12 (1) (2002) 1520–1523.
[16] S.W. Van Sciver, Helium Cryogenics, Plenum Press, New York, 1986.
[17] J. Crank, Free and Moving Boundary Problems, Oxford University Press, Oxford, 1984.
[18] V.R. Voller, C.R. Swaminathan, Fixed grid techniques for phase change problem: a review, Int. J. Numer. Meth. Engng. 30 (1990) 875–898.
[19] J.W. Cahn, J.E. Hillard, Free energy of a nonuniform system. I. Interface free energy, J. Chem. Phys. 28 (1958) 258–267.
[20] V. Voller, M. Cross, Accurate solutions of moving boundary problems using the enthalpy method, Int. J. Heat Mass Transfer 24 (1981) 545–556.
[21] C. de Boor, Good approximation by splines with variables knots, Lecture Notes in Mathematics, 363, Springer-Verlag, New York, 1974.
[22] E.A. Dorfi, L. O'c. Drury, Simple adaptive grids for 1-D initial value problems, J. Comput. Phys. 69 (1987) 175–195.
[23] K. Farrell, L. O'c Drury, An explicit, adaptive grid algorithm for one-dimensional initial value problems, Appl. Numer. Math. 26 (1) (1998) 3–12.

[24] J.A. Mackenzie, M.L. Robertson, The numerical solution of one-dimensional phase change problems using an adaptive moving mesh method, J. Comput. Phys. 161 (2000) 537–557.

[25] V. Arp, R. McCarty, thermophysical properties of Helium-4 from 0.8 to 1500 K with pressure to 2000 MPa, NITS Tech Note 1334, US Government Printing Office, Washington, USA, 1999 (rev).